Experimental and Theoretical Studies of the Reaction of the Phenyl Radical with Methane

I. V. Tokmakov, J. Park, S. Gheyas, and M. C. Lin*

Department of Chemistry, Emory University, Atlanta, Georgia 30322

Received: July 23, 1998; In Final Form: March 16, 1999

The kinetics of the metathetical reaction of phenyl radical with methane has been studied theoretically and experimentally. The rate constants determined by two complementary methods, pyrolysis/Fourier transform infrared spectrometry and pulsed laser photolysis/mass spectrometry in the temperature range 600−980 K, give the Arrhenius equation: $k_1 = 10^{12.78 \pm 0.13} \exp[(-6201 \pm 225)/T]$ cm^3/(mol s). At the best theoretical level employed (G2M(CC,MP2)), the barrier for the reaction at 0 K is $E_1^0 = 9.3$ kcal/mol. The rate constant k_1 calculated from theoretical molecular parameters fits experimental data if the barrier height is increased to 10.5 kcal/mol. The fitted barrier is well within the 2−3 kcal/mol accuracy of the G2M method for the present open-shell, seven-heavy-atom system. Because of the relatively high reaction barrier and the predicted high imaginary frequency (1551 cm^{-1}), tunneling corrections resulted in a significant enhancement in the calculated rate constant, 150% at 500 K and 7% at 2000 K. The theoretical result also correlates well with recently reported shock-tube data measured in the temperature range 1050−1450 K by UV absorption spectrometry. Kinetic analysis of the toluene formation data obtained from the photolysis of acetophenone without and with added H_2 and CH_4 gave the rate constant for the recombination of CH_3 and C_6H_5, $k_2 = (1.38 \pm 0.08) \times 10^{13} \exp[-(23 \pm 36)/T]$ cm^3/(mol s) for the temperature range 300−980 K.

1. Introduction

The phenyl radical plays an important role in the formation of polycyclic aromatic hydrocarbons in the combustion of fossil fuels. To provide the combustion community with much needed rate constants for kinetic modeling of soot formation chemistry, we have recently carried out a series of studies on the kinetics of C_6H_5 radical reactions[1−5] by the cavity ringdown spectrometry (CRDS) technique,[6,7] which is effective for reactions with bimolecular rate constants $\geq 10^8$ cm^3/(mol s). For slower metathetical processes, such as $C_6H_5 + H_2$, we have developed a complementary method based on pulsed laser photolysis/mass spectrometry (PLP/MS)[8,9] using the supersonic sampling technique employed by Saalfeld and co-workers.[10,11] In addition, we have utilized conventional pyrolysis/Fourier transform infrared spectrometry (P/FTIRS), measuring the absolute yield of C_6H_6 in the pyrolysis of nitrosobenzene, with and without added NO, in the presence of a large excess of H_2.[9] The results of these two complementary studies (which extended the experimental temperature up to 1000 K from the maximum temperature of 523 K by CRDS) for $C_6H_5 + H_2$ were found to be in excellent agreement with the shock-tube data of Heckmann et al.[12] as well as with our theoretically predicted values.[13]

In this work, we have employed both P/FTIRS and PLP/MS techniques for determination of the rate constant for the analogous metathetical process, $C_6H_5 + CH_4 \rightarrow C_6H_6 + CH_3$, which has been shown to be qualitatively slower than the H_2 reaction.[12] Additionally, we have carried out a comprehensive series of ab initio molecular orbital (MO) calculations following the framework of the G2M method[14] employed in our previous study of the $C_6H_5 + H_2$ reaction. Both theoretical and experimental results will be discussed and compared with the existing scarce kinetic data on the $C_6H_5 + CH_4$ reaction.[12,15]

* Corresponding author. E-mail address: chemmcl@emory.edu.

2. Experimental Procedure

The experimental procedures for both P/FTIRS and PLP/MS methods have been described in detail before.[8,9] Hence, only a brief summary of each method is presented below.

P/FTIRS. In this technique, C_6H_5NO was used as a phenyl radical source. C_6H_5NO was pyrolyzed to generate the C_6H_5 radical, and its reactivity toward CH_4 was studied in the 598−653 K range by FTIRS. Absorption peaks at 673.199 and 680.915 cm^{-1}, properly deconvoluted, were employed for the determination of C_6H_6 and C_6H_5NO, respectively.

Figure 1 shows a typical concentration vs time plot for the formation of C_6H_6 and the decay of C_6H_5NO. The corresponding curves represent kinetically modeled values. The rate constants for the reaction of C_6H_5 with CH_4, the sole source of C_6H_6, obtained by modeling are summarized in Table 1.

PLP/MS. The pulsed photolysis of $C_6H_5COCH_3$ at 193 nm was employed as the C_6H_5 radical source. The mole fraction of $C_6H_5COCH_3$ was typically <0.3% and those of He (which carried the C_6H_5 radical source into the Saalfeld type quartz reactor) and CH_4 were varied in the range 15%−85%. The photolytic conversion of acetophenone was in the range 20−45%. To determine the amount of C_6H_5 formed under the present conditions, NO was used as the C_6H_5 radical scavenger with $[NO]/[C_6H_5COCH_3] > 200$. NO titration revealed that on average 62−80% of the dissociated acetophenone produced the C_6H_5 radical in our experimental conditions depending on photolytic laser energy (typically 30−40 mJ) and acetophenone concentration. The reactants and the products of the photoinitiated reaction were supersonically sampled and ionized by electron impact ionization.

Mechanistically, although the missing 20−38% of the products from the photofragmentation of $C_6H_5COCH_3$ has not been quantitatively identified due to mass overlap with the fragment ions of the parent molecule, it is known experimentally

10.1021/jp983140s CCC: $18.00
Published on Web 04/24/1999

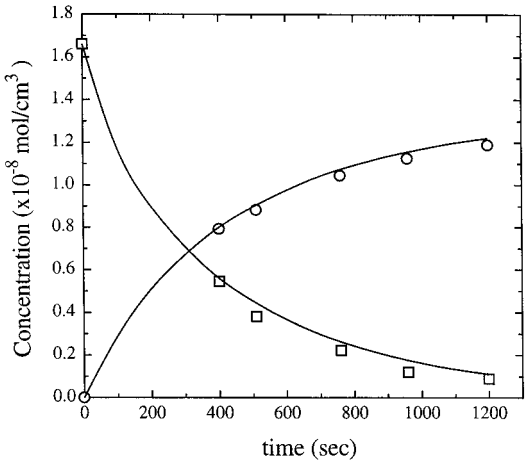

Figure 1. Time-resolved concentration profiles of C_6H_5NO decay (□) and C_6H_6 formation (○) in a P/FTIRS experiment at 653 K. Curves are the modeled results. Reaction conditions are given in Table 1. All C_6H_6 yields were enlarged by a factor of 2.

TABLE 1: Experimental Conditions[a] and Modeled Rate Constants in the P/FTIRS Experiment for the Reaction of C_6H_5 + CH_4 at the Temperatures Studied

temp (K)	$[C_6H_5NO]_o$	$[NO]_o$	$[CH_4]_o$	$k/10^8$ (cm^3/mol s)[b]
598	0.58	0	749.42	1.87 ± 0.13
603	0.58	0	749.42	1.49 ± 0.11
613	0.68	2.12	747.20	1.90 ± 0.11
623	0.47	1.86	747.67	2.00 ± 0.19
633	0.68	2.12	747.20	2.37 ± 0.19
643	0.47	1.86	747.67	2.76 ± 0.14
653	0.68	2.12	747.20	2.40 ± 0.24

[a] The concentrations are given in Torr. [b] Typically 3−5 runs were carried out for each temperature. The uncertainty represents 1σ.

that those fragments **do not** lead to C_6H_6 or $C_6H_5CH_3$ in their subsequent reactions. To fully quantify the amounts of C_6H_5 and CH_3 radicals formed in the initial fragmentation reaction in the absence of CH_4, we measured the yields of C_2H_6 and $C_6H_5CH_3$ concurrently, which allowed us to quantify CH_3 and C_6H_5 concentrations at the same time. As shown in Table 2, both C_2H_6 and $C_6H_5CH_3$ yields can be quantitatively modeled and the rate constant for $C_6H_5 + CH_3$ (k_2) thus obtained agrees with those acquired in the H_2 and CH_4 added studies.

As mentioned in our earlier paper on $C_6H_5 + H_2$,[9] the major products measured in the photolysis of $C_6H_5COCH_3$ were C_6H_5-CH_3, C_2H_6, and $C_{12}H_{10}$ with a trace amount of C_6H_6. Addition of CH_4 to the system resulted in a noticeable increase in the yield of C_6H_6. Table 2 summarizes the experimental conditions employed and the yields of C_6H_6 and $C_6H_5CH_3$ measured in the PLP/MS experiment. Kinetic modeling of the absolute concentrations of C_6H_6 and $C_6H_5CH_3$ provided the rate constants for the following two key reactions:

$$C_6H_5 + CH_4 \rightarrow C_6H_6 + CH_3 \quad (1)$$

$$C_6H_5 + CH_3 \rightarrow C_6H_5CH_3 \quad (2)$$

3. Computational Methods

The equilibrium geometries of the reactants, transition state, and products were found by the hybrid density functional B3LYP method (Becke's three parameter nonlocal exchange functional[16] with the nonlocal correlation functional of Lee, Yang and Parr[17]) with the 6-311++G(d,p) basis set.[18] Vibrational frequencies calculated at the same level of theory were employed for zero-point energy (ZPE) correction, characterization of the nature of stationary points, and canonical transition state theory (CTST)[19] calculation of the rate constant. All the energies herein include ZPE corrections. For a more accurate evaluation of the energetics of the reaction, higher level single point calculations were carried out on the optimized geometries. The two computational schemes[14] used in the present study calculate a series of CCSD(T), MP4(SDTQ), and MP2 energies with various basis sets to approximate CCSD(T)/6-311+G(3df,-2p)//B3LYP/6-311++G(d,p) energies with an additional "higher level correction" (HLC) based on the number of paired and unpaired valence electrons. The first model G2M(cc,MP2) calculates the base energy E_{bas} at the MP4/6-311G(d,p) level of theory and improves it with the expanded basis set (ΔE(+3df2p)) and coupled cluster (ΔE(cc)) corrections and HLC:

$$E[\text{G2M(cc,MP2)}] = E_{bas} + \Delta E(+3\text{df2p}) + \Delta E(\text{cc}) + \Delta E(\text{HLC,cc,MP2}) + \text{ZPE} \quad \text{(I)}$$

where

$$\Delta E(+3\text{df2p}) = E[\text{MP2/6-311+G(3df,2p)}] - E[\text{MP2/6-311G(d,p)}]$$

$$\Delta E(\text{cc}) = E[\text{CCSD(T)/6-31G(d,p)}] - E[\text{PMP4/6-31G(d,p)}]$$

$$\Delta E(\text{HLC,cc,MP2}) = -0.00505n_\beta - 0.00019n_\alpha \text{ (in Hartree)}$$

where n_α and n_β are the number of α and β valence electrons ($n_\alpha \geq n_\beta$).

The second model G2M(CC,MP2) differs only in the calculation of the coupled cluster correction and the empirical coefficient for n_β in the HLC. The G2M(CC,MP2) model uses ΔE(CC) calculated with the triple-ζ 6-311G(d,p) basis set:

$$\Delta E(\text{CC}) = E[\text{CCSD(T)/6-311G(d,p)}] - E_{bas}$$

resulting in the cancelation of E_{bas} in eq I to yield the final expression E[G2M(CC,MP2)] = E[CCSD(T)/6-311G(d,p)] + ΔE(+3df2p) + ΔE(HLC,CC,MP2) + ZPE, with ΔE(HLC,CC,-MP2) = $-0.00530n_\beta - 0.00019n_\alpha$.

We should note that in the reaction studied here the numbers n_α and n_β are the same for the reactants, transition state, and products, which results in the cancelation of the HLCs for all relative energies. Therefore, the calculation of the reaction barrier and enthalpy does not involve any empirical parameters.

For all the molecular orbital calculations the GAUSSIAN94 program package[20] was used.

4. Results and Discussion

A. Experimental Kinetic Data. *Evaluation of k_1 and k_2.* As mentioned in the preceding section, two complementary techniques were employed to measure the rate constant for the C_6H_5 + CH_4 reaction using widely different conditions. With the P/FTIRS technique the absolute yields of C_6H_6 formed by the abstraction reaction were measured under atmospheric pressure conditions as functions of time and temperature using different C_6H_5NO and NO mixtures diluted with CH_4. NO was added to retard the rate of C_6H_5NO decomposition in order to reach higher temperatures required for the slow reaction of C_6H_5 with CH_4. Figure 1 shows a typical set of time-resolved C_6H_6 formation and C_6H_5NO decay data. Solid curves presented in the figure correspond to the kinetically modeled values using the CHEMKIN/SENKIN program[21] with the mechanism em-

TABLE 2: Experimental Conditions,[a] Product Yields,[b] and Modeled Rate Constants[c] in the PLP/MS Experiment at the Temperatures Studied

						$[C_2H_6]_t$		$[C_6H_6]_t$			$[C_6H_5CH_3]_t$		
temp (K)	P (Torr)	$[C_6H_5COCH_3]_0$	$[C_6H_5]_0$	$[He]_0$	$[CH_4]_0$	exp[d]	model	exp	model	$k_1/10^9$	exp	model	$k_2/10^{13}$
303*	3.00	2.56	1.29	2993.6		0.43	0.43				0.33	0.35	1.39
391*	3.00	2.28	0.74	2995.7		0.25	0.23				0.20	0.19	1.28
444*	3.00	2.53	1.02	2994.4		0.33	0.32				0.27	0.27	1.24
587*	3.00	2.25	0.69	2995.7							0.19	0.19	1.23
706*	3.00	2.83	0.92	2994.4							0.30	0.30	1.29
737	3.07	5.95	1.65	440.5	2605.4			0.25	0.24	1.54	0.67	0.65	1.34
785*	3.00	3.01	0.49	2995.5							0.14	0.14	1.41
798	3.06	6.10	1.50	441.5	2611.5			0.31	0.31	2.75	0.65	0.65	1.48
848	3.06	6.19	1.41	439.0	2596.9			0.41	0.40	3.84	0.59	0.58	1.59
907	3.07	5.52	1.78	440.5	2605.8			0.53	0.52	5.91	0.63	0.64	1.30
933	3.05	5.09	1.91	440.6	2606.1			0.58	0.58	7.25	0.67	0.66	1.48
965	3.07	5.65	1.35	442.0	2615.4			0.54	0.55	8.47	0.47	0.46	1.40
984	3.08	5.32	1.68	442.8	2619.8			0.60	0.60	8.85	0.60	0.60	1.52

[a] All concentrations are given in mTorr. [b] Product yields were measured at $t = 5$ ms (denoted by *) or 15 ms at their plateaus. Typically 2−3 runs were carried out for each temperature. [c] In units of cm^3/(mol s). [d] The yields of C_2H_6 decreased rapidly with temperature because of the strong negative T dependence and the low-pressure employed.

TABLE 3: Reactions and Rate Constants[a] Used in the Modeling of the $C_6H_5 + CH_4$ Reaction in the P/FTIRS Experiment

	reactions	A	n	E_a	ref[c]
	Key Reactions				
1.	$C_6H_5 + CH_4 \rightarrow C_6H_6 + CH_3$	6.03E+12[b]	0.0	12321	this work
2.	$C_6H_5 + CH_3 \rightarrow C_6H_5CH_3$	1.38E+13	0.0	46	this work
3.	$C_6H_5 + C_6H_5 \rightarrow C_{12}H_{10}$	1.39E+13	0.0	111	
4.	$CH_3 + CH_3 (+M) \rightarrow C_2H_6 (+M)$ LOW/1.770E+50 −9.670 6220.00/ TROE/0.5325 151.00 1038.00 4970.00/ CH_4/2.0/ C_2H_6/3.0/ AR/ 0.7/ NO/1.5 C_6H_6/3.0 C_6H_5NO/5.0/	2.12E+16	−1.0	620	
5.	$C_6H_5NO \leftrightarrow C_6H_5 + NO$	1.42E+17	0.0	55060	
6.	$C_6H_5 + C_6H_5NO \rightarrow C_{12}H_{10}NO$	4.90E+12	0.0	−68	
	Minor Reactions				
7.	$CH_3 + C_6H_5CH_3 \rightarrow CH_4 + C_7H_7$	5.50E+11	0.0	12000	
8.	$C_7H_7 + C_6H_5 \rightarrow C_{13}H_{12}$	1.19E+13	0.0	220	22
9.	$C_7H_7 + C_7H_7 \rightarrow C_{14}H_{14}$	2.51E+11	0.4	0	29
10.	$C_7H_7 + NO \rightarrow C_7H_7NO$	5.73E+12	0.0	0	30
11.	$C_6H_5 + C_6H_5CH_3 \rightarrow C_6H_6 + C_7H_7$	4.15E-03	4.5	−1590	26
12.	$C_{12}H_{10}NO \rightarrow C_6H_5NO + C_6H_5$	5.00E+14	0.0	45000	
13.	$C_6H_5 + C_{12}H_{10}NO \rightarrow C_{12}H_{10}N + C_6H_5O$	1.00E+12	0.0	0	
14.	$C_6H_5 + C_6H_5NO \rightarrow C_{12}H_{10} + NO$	5.00E+12	0.0	4500	
15.	$C_{12}H_{10}N + NO \rightarrow C_{12}H_{10}NNO$	1.00E+13	0.0	0	

[a] Rate constants are defined by $k = AT^n \exp(-E_a/RT)$ and in units cm^3, mol, and s; E_a is in units of cal/mol. [b] Read as 6.03×10^{12}. [c] Reference 9 unless otherwise noted.

ployed for the $C_6H_5NO/NO/H_2$ system,[9] after a minor modification by replacing H_x ($x = 1, 2$) reactions with CH_y ($y = 3, 4$) processes (see Table 3). Table 1 summarizes the modeled rate constant as a function of temperature for the CH_4 reaction obtained by averaging the kinetically modeled values at different resident times. The Arrhenius plot for the rate constant is given in Figure 2.

The key reactions occurring in this system are

$$C_6H_5 + CH_4 \rightarrow C_6H_6 + CH_3 \qquad (1)$$

$$C_6H_5NO \leftrightarrow C_6H_5 + NO \qquad (5, -5)$$

$$C_6H_5 + C_6H_5NO \rightarrow C_{12}H_{10}NO \qquad (6)$$

as illustrated in Figure 3 by the results of sensitivity analyses for the $C_6H_5NO/NO/CH_4$ system. The reactions with sensitivity coefficients less than 0.01 are not included in the figure. Figure 4 shows the sensitivity of the reactant and product concentration profiles to the different values of k_1 (Figure 4a) and k_5 (Figure 4b) by varying them up and down by a factor of 2. As shown in the figure, the concentration profiles of the reactant and product are quite sensitive to the value of k_1. For reaction 5 (Figure 4b), we used a factor of 2 higher or lower value of k_5 and obtained a relatively close fitting of the C_6H_6 concentration profile by varying the value of k_1 by a factor of 0.7 or 1.4, respectively, but we were not able to quantitatively account for the C_6H_5NO profile. We should emphasize, however, that the values of k_5 and k_{-5} have been very well-established in our recent kinetic studies.[22,23] For reaction 3, $C_6H_5 + C_6H_5 \rightarrow C_{12}H_{10}$, Heckmann et al.[12] reported the rate constant as 5.7×10^{12} cm^3/(mol s) near 1000 K, which is 2 times lower than our result, $k_3 = 1.39 \times 10^{13} \exp(-55/T)$ cm^3/(mol s),[8] extrapolated to their temperature region, whereas Horn et al.[24] reported for the same temperature regime a value that is twice higher than ours. As shown in Figure 4c, the use of the higher or lower value of k_3 affects very little the reactant concentration or the product yield. We also examined the sensitivity of the reactant and product yields to the values of k_6, but no significant changes were observed in their yields for the twice higher or lower value of k_6.

In the PLP/MS experiment at higher temperatures, $C_6H_5COCH_3$ was employed as the C_6H_5 radical source as in the $C_6H_5 + H_2$ study.[9] The initial concentration of C_6H_5 produced in the present photolysis, as mentioned before, could be reliably

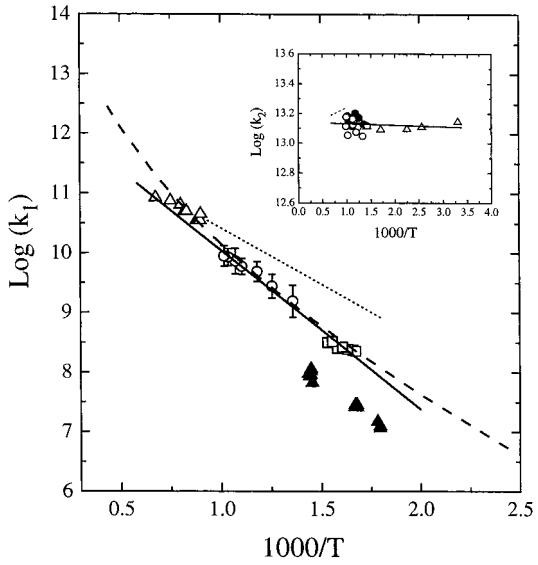

Figure 2. Arrhenius plot of the rate constant for the $C_6H_5 + CH_4$ reaction: (△) ref 12; (▲) ref 15 using the rate constant for the recombination of C_6H_5 given in ref 8; (○) this work by PLP/MS; (□) this work by P/FTIRS; (dotted line) ref 12; (dashed curve) our predicted value with tunneling corrections using $E_1^0 = 10.5$ kcal/mol; (solid line) the result of a weighted least-squares analysis for our P/FTIRS and PLP/MS data. Inset: Arrehnius plot of the modeled rate constant for the $C_6H_5 + CH_3$ reaction: (●) ref 9; (△) this work without CH_4; (○) this work with CH_4 added; (dotted line) the recommended result of Tsang and Kiefer (ref 25).

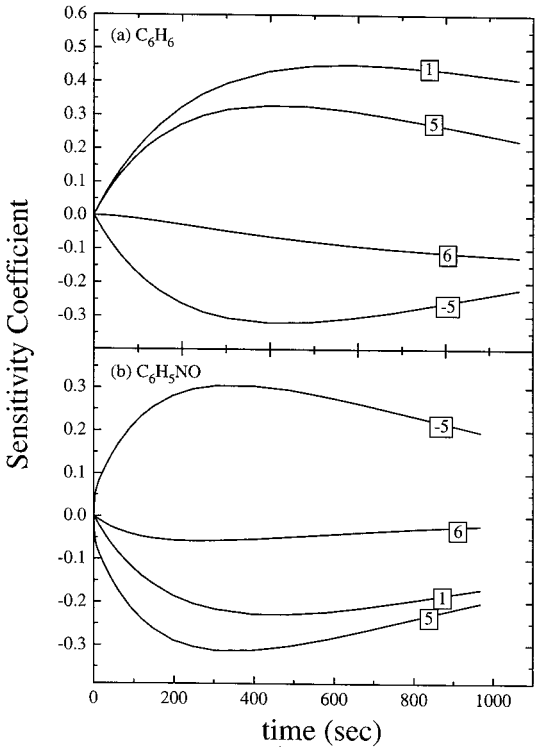

Figure 3. Sensitivity analyses for C_6H_6 (a) and C_6H_5NO (b) at 653 K in the P/FTIRS experiment.

measured by the amount of C_6H_5NO formed in the presence of excess NO as the radical scavenger.

The measurement of toluene, one of the major products formed in the pulsed laser photolysis of $C_6H_5COCH_3$ in the presence or absence of CH_4, is very useful because its formation results solely from the recombination of C_6H_5 with CH_3, allowing us to reliably monitor the concentration of the C_6H_5 radical. Since both radicals are expected to be formed with equal concentrations initially, as suggested by our quantitative modeling of C_2H_6 and $C_6H_5CH_3$ yields in the absence of CH_4 (see Table 2), the concurrent modeling of the yields of C_6H_6 and $C_6H_5CH_3$ with an excess amount of CH_4 should provide reliable rate constants for reactions 1 and 2. The modeled values using the mechanism given in Table 4 are summarized in Table 2 and graphically presented in Figure 2, together with P/FTIRS and other existing data[12,15] for comparison with the theoretically predicted result (to be discussed later). A weighted least-squares analysis of the two sets of experimental data covering 600−980 K gives $k_1 = 10^{12.78\pm0.13} \exp[-(6201 \pm 225)/T]$ cm^3/(mol s).

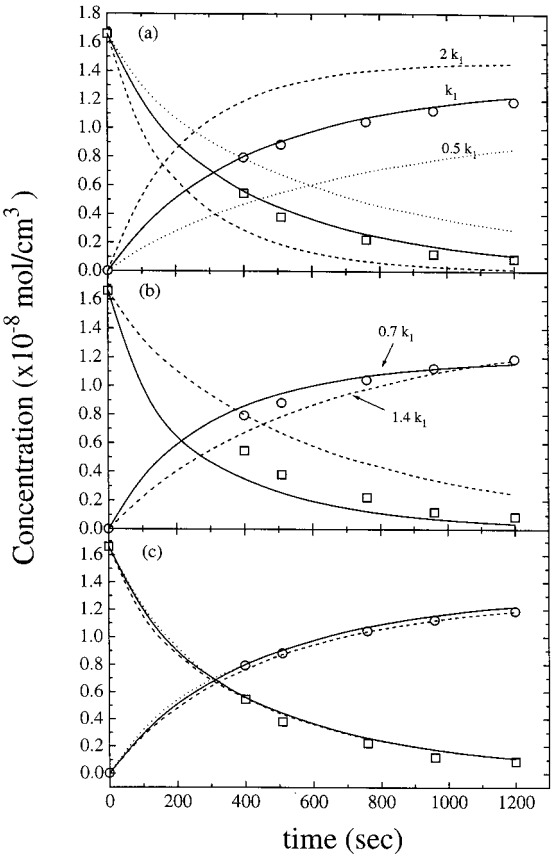

Figure 4. Sensitivities of k_1 (a), k_5 (b), and k_3 (c) to C_6H_5NO decay (□) and C_6H_6 formation (○). (b) We used $2k_5$ (solid curve) or $0.5k_5$ (dashed curve) for the modeling and varied k_1 in order to fit to concentration profiles. (c) Solid curve using our k_3;[8] dashed curve using k_3 of Horn et al.;[24] dotted curve using k_3 of Heckmann et al.[12] All C_6H_6 yields were enlarged by a factor of 2.

For k_2, it is reassuring that the values determined in the present work (shown in the inset of Figure 2) agree closely with those reported earlier from the $C_6H_5 + H_2$ study[9] as well as with Kiefer and Tsang's estimation based on the $C_6H_5CH_3$ dissociation kinetics.[25] A least-squares analysis of k_2 obtained from measurements with and without H_2 and CH_4 added gave $k_2 = 10^{13.14 \pm 0.03} \exp[-(23 \pm 36)/T]$ cm^3/(mol s).

For reaction 1, we have included in Figure 2 two existing sets of kinetic data reported by Duncan and Trotman-Dickenson[15] employing steady-state UV photolysis of $C_6H_5COCH_3$ in the presence of CH_4 and by Heckmann et al.[12] using the shock-tube/UV absorption spectroscopy carried out in the temperature range 1050−1450 K. The result of Duncan and Trotman-Dickenson[15] was evaluated with reference to the C_6H_5 recombination reaction, whose rate constant was assumed to be $k_3 = 1 \times 10^{14}$ cm^3/(mol s), independent of temperature. We rescaled

TABLE 4: Reactions and Rate Constants[a] Used in the Modeling of the $C_6H_5 + CH_4$ Reaction in the PLP/MS Experiment

	reactions	A	n	E_a	ref[c]
	Key Reactions				
1.	$C_6H_5 + CH_4 \rightarrow C_6H_6 + CH_3$	6.03E+12[b]	0.0	12321	this work
2.	$C_6H_5 + CH_3 \rightarrow C_6H_5CH_3$	1.38E+13	0.0	46	this work
3.	$C_6H_5 + C_6H_5 \rightarrow C_{12}H_{10}$	1.39E+13	0.0	111	
4.	$CH_3 + CH_3 (+M) \rightarrow C_2H_6 (+M)$ LOW /1.770E+50 −9.670 6220.00/ TROE/0.5325 151.00 1038.00 4970.00/ H_2/2.00 CH_4/2.0/ CO/1.5/ C_2H_6/3.0/ He/ 0.7/ C_6H_6/3.0 $C_6H_5COCH_3$/5.0/	2.12E+16	−1.0	620	
	Minor Reactions				
7.	$CH_3 + C_6H_5CH_3 \rightarrow CH_4 + C_7H_7$	5.50E+11	0.0	12000	
8.	$C_7H_7 + C_6H_5 \rightarrow C_{13}H_{12}$	1.19E+13	0.0	220	22
9.	$C_7H_7 + C_7H_7 \rightarrow C_{14}H_{14}$	2.51E+11	0.4	0	29
11.	$C_6H_5 + C_6H_5CH_3 \rightarrow C_6H_6 + C_7H_7$	4.15E−03	4.5	−1590	26
16.	$C_6H_5 + C_6H_5COCH_3 \rightarrow C_6H_6 + C_6H_5COCH_2$	4.15E−03	4.5	−1590	*d*
17.	$C_6H_5CO \rightarrow C_6H_5 + CO$	3.98E+14	0.0	28404	
18.	$CH_3 + C_6H_5COCH_3 \rightarrow CH_4 + C_6H_5COCH_2$	5.01E+10	0.0	7400	
19.	$C_6H_5 + C_6H_5COCH_3 \rightarrow C_{12}H_{10}COCH_3$	1.00E+12	0.0	4000	
20.	$C_6H_5COCH_2 + CH_3 \rightarrow C_6H_5COC_2H_5$	5.00E+12	0.0	0	
21.	$C_6H_5COCH_2 + C_6H_5 \rightarrow C_{12}H_{10}COCH_2$	1.19E+13	0.0	220	
22.	$C_6H_5COCH_2 + C_6H_5COCH_2 \rightarrow (C_6H_5COCH_2)_2$	2.51E+11	0.4	0	
23.	$C_6H_5COCH_2 \rightarrow C_6H_5 + CH_2CO$	4.00E+14	0.0	29400	
24.	$C_{12}H_{10}COCH_3 \rightarrow C_{12}H_{10} + CH_3CO$	1.00E+08	0.0	0	
25.	$CH_3 + CH_3CO \rightarrow CH_3COCH_3$	4.04E+15	−0.8	0	
26.	$CH_3CO (+M) \rightarrow CH_3 + CO (+M)$	8.74E+42	−8.6	22420	
27.	$C_6H_5 + H_2 \rightarrow C_6H_6 + H$	5.72E+04	2.43	6276	
28.	$2H + M \rightarrow H_2 (+M)$	1.00E+18	−1.0	0	
29.	$C_6H_5 + H \rightarrow C_6H_6$	7.80E+13	0.0	0	
30.	$CH_3 + H_2 \rightarrow CH_4 + H$	2.89E+02	3.12	8710	
31.	$C_6H_5CH_3 + H \rightarrow C_7H_7 + H_2$	3.98E+02	3.44	3120	
32.	$C_6H_5CH_3 + H \rightarrow C_6H_6 + CH_3$	5.78E+13	0.0	8090	

[a] Rate constants are defined by $k = AT^n \exp(-E_a/RT)$ and in units cm^3, mol, and s; E_a is in the units of cal/mol. [b] Read as 6.03×10^{12}. [c] Reference 9 unless otherwise noted. [d] Assumed on the basis of the reaction rate of (11).

their CH_4 abstraction rate constant by using our reported C_6H_5 recombination rate constant $k_3 = 1.39 \times 10^{13} \exp(-55/T)$ cm^3/(mol s).[8] It should be mentioned that the same set of data was also utilized by Heckmann et al.[12] to evaluate the Arrhenius expression for the reaction using their reported C_6H_5 recombination rate, $k_3 = 5.7 \times 10^{12}$ cm^3/(mol s), which is expected to result in a slightly greater downward shift from Duncan and Trotman-Dickenson's original value. However, the shift was in fact made in the opposite, upward direction, which resulted in the final Arrhenius expression $k_1 = 10^{12.3} \exp(-4330/T)$ cm^3/(mol s) (see the dashed line in Figure 2). The rescaled values (given by the solid triangles in the figure) deviate significantly from the present result and Heckmann's high-temperature data, which are qualitatively in reasonable agreement.

Figure 5 shows the results of sensitivity analyses for C_6H_6 and $C_6H_5CH_3$ products in a PLP/MS experiment at 933 K. The key reactions occurring in this system, aside from the major $C_6H_5 + CH_4$ (1) abstraction process of interest, are the recombination reactions ($C_6H_5 + CH_3$ (2), $C_6H_5 + C_6H_5$ (3), and $CH_3 + CH_3$ (4), which has a much smaller effect on the C_6H_6 and $C_6H_5CH_3$ yields). As shown in the figure, the formation of C_6H_6 is most positively affected by reaction 1 and negatively influenced by its competitive reactions 2 and 3, while the formation of $C_6H_5CH_3$ is most positively affected by reaction 2 and negatively influenced by its competitive reactions 1 and 3. The use of the higher[24] or lower[12] values of k_3, as referred to earlier, increases or lowers the modeled values of k_1 by as much as 80% because of the strong competition between reactions 1 and 3. The smaller k_3 of Heckmann et al.[12] would reduce the value of k_1 by about 80%, resulting in a greater deviation from their recommended expression, $k_1 = 10^{12.3} \exp(-4330/T)$ cm^3/(mol s);[12] the smaller values of k_1 would also become inconsistent with our theoretically predicted result and the P/FTIRS kinetic data, which are not affected by the use of different k_3 values, as discussed earlier.

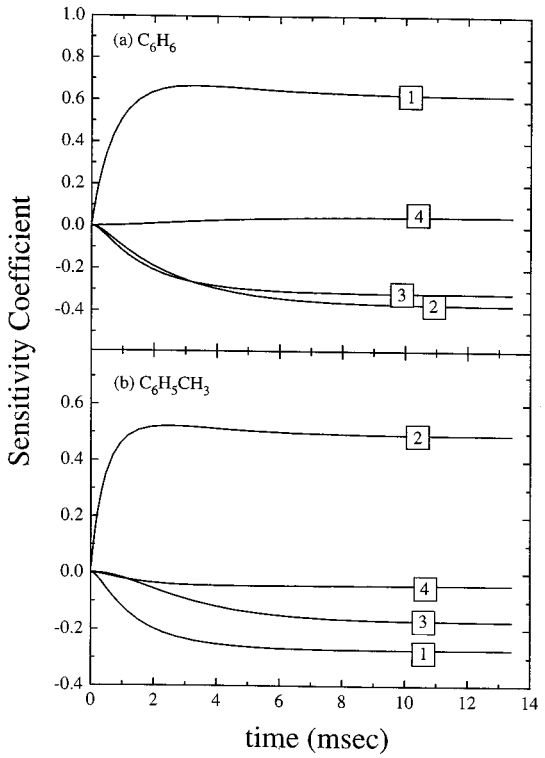

Figure 5. Sensitivity analyses C_6H_6 (a) and $C_6H_5CH_3$ (b) at 933 K in the PLP/MS experiment. Conditions are given in Table 2.

Validity of k_{-1}. Complementary to the experimental kinetic data for reaction 1, the rate constant for its reverse process, $CH_3 + C_6H_6 \rightarrow CH_4 + C_6H_5$, has been determined by Krech and

Price,[27] $k_{-1} = 6.3 \times 10^{10} \exp(-4680/T)$ cm^3/(mol s), in a flow tube study employing either dimethylmercury or dimethylcadmium as the CH_3 radical source. The rate constant was measured at temperatures 744−800 K by a relative rate method using the recombination of CH_3 radicals as a reference reaction. Zhang et al.[28] obtained a much different rate constant expression, $k_{-1} = 2 \times 10^{12} \exp(-7580/T)$ cm^3/(mol s), from their steady-state analysis of the CH_4 formed in the pyrolysis of C_2H_4 with and without C_6H_6 added in the temperature range 650−770 K at 220−380 Torr pressure. These results, particularly that of Krech and Price,[27] which has a significantly lower activation energy than our estimated barrier, 18.1 kcal/mol at 0 K ($E_{-1}^0 = E_1^0 - \Delta H_0^0$ using an experimental $\Delta H_0^0 = -8.8$ kcal/mol and the best theoretical value of $E_1^0 = 9.3$ kcal/mol), give rise to a forward rate constant that is about a factor of 10 higher than ours.

To understand this large deviation, we have attempted to kinetically model the relative rate constants obtained by Krech and Price based on the yields of CH_4 and C_2H_6 in their pyrolysis of $(CH_3)_2M$ (M = Hg or Cd) in the presence of excess amounts of C_6H_6. The CH_4 and C_2H_6 formed in the system were assumed to have derived exclusively from the reactions

$$CH_3 + C_6H_6 \rightarrow CH_4 + C_6H_5 \qquad (-1)$$

$$CH_3 + CH_3 \rightarrow C_2H_6 \qquad (4)$$

which gives the relative rate constant:

$$\frac{k_{-1}}{k_4^{1/2}} = \frac{R_{CH_4}}{[C_6H_6]R_{C_2H_6}^{1/2}} \qquad (II)$$

where R_X represents the initial rate of formation of the product X. The relative rate constant given by eq II can be readily modeled by using the known kinetics for the decomposition of $(CH_3)_2M$, $CH_3 + (CH_3)_2M$, and other C_1 and C_2 reactions relevant to the system.[29] The results of our modeling indicated that the reported relative rate constants are consistent with the calculated concentration ratios given by the right-hand side of eq II if CH_4 was produced primarily by reaction −1 and the k_{-1} value reported by these authors was used. However, if the catalytic effect of C_7H_9 (methylcyclohexadienyl) radical, formed by the $CH_3 + C_6H_6$ addition reaction, was introduced with our theoretically predicted rate constants[30] for the reactions

$$CH_3 + C_6H_6 \leftrightarrow C_7H_9$$

$$CH_3 + C_7H_9 \rightarrow CH_4 + C_7H_8$$

$$C_7H_9 \rightarrow C_7H_8 + H$$

the yields of CH_4 and C_2H_6 were found to be significantly affected by secondary and tertiary reactions involving H, CH_3, and C_2H_5. In this regard, we have previously pointed out that the apparent rate constant reported for the analogous reaction $H + C_6H_6 \rightarrow H_2 + C_6H_5$ below 1000 K could be attributed entirely to the C_6H_7-catalyzed reaction, similar to the one given above, $H + C_6H_6 \leftrightarrow C_6H_7$, $H + C_6H_7 \rightarrow H_2 + C_6H_6$.[13]

We have also kinetically modeled the production of CH_4 in the complex $C_2H_4-C_6H_6$ system studied by Zhang et al.[28] The result of our modeling revealed that the apparent enhancement in the yields of CH_4 upon the addition of C_6H_6 to the C_2H_4 system could not have resulted directly from the assumed reaction (−1). In fact, the employment of both our k_1 and Zhang's k_{-1} in the modeling gave essentially the same low CH_4 yields using a reasonable mechanism, which comprised all of their suggested reactions leading to the formation of CH_4. The C_2H_4 system is, perhaps, too complicated for a reliable and clean determination of the elementary kinetics of an unsaturated hydrocarbon molecule such as C_6H_6, which may undergo many unknown secondary reactions producing CH_x ($x = 3$ and 4). We have, therefore, concluded that the values of k_{-1}, reported by Krech and Price[27] and by Zhang et al.,[28] are not reliable and also inconsistent with the large reverse barrier predicted by our high-level ab initio MO calculations.

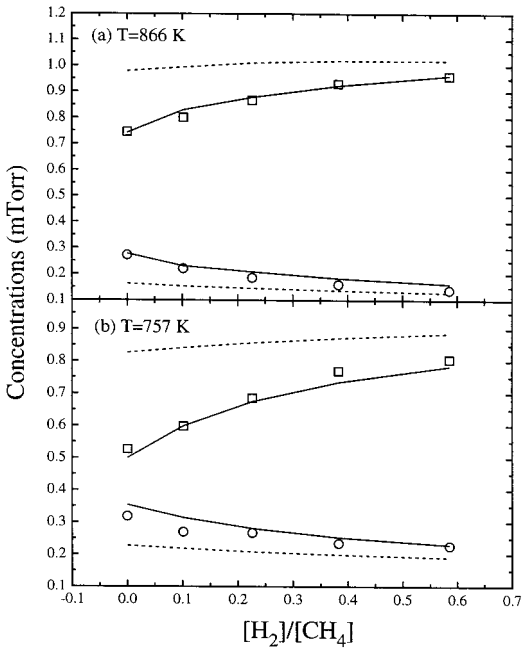

Figure 6. Concentration profiles of C_6H_6 (□) and $C_6H_5CH_3$ (○) as a function of $[H_2]/[CH_4]$ at the total pressure of 10 Torr. Reaction conditions: (a) $[C_6H_5COCH_3]_0 = 1.57$, $[C_6H_5]_0 = 1.27$, [He] = 837.1; (b) $[C_6H_5COCH_3]_0 = 1.58$, $[C_6H_5]_0 = 1.26$, [He] = 837.1. All concentrations are given in mTorr. Solid curves were predicted values using the mechanism presented in Table 4 and rate constants as given. For the dotted curves, k_1 was replaced by that reported by Heckmann et al.[12]

Test for the Validity of Our k_1. In view of the noticeable difference between our rate constant for the $C_6H_5 + CH_4$ reaction, $k_1 = 10^{12.78} \exp(-6201/T)$ cm^3/(mol s), and that of Heckmann et al., $k_1 = 10^{12.3} \exp(-4330/T)$ cm^3/(mol s),[12] in the temperature range 300−1000 K, as also graphically shown in Figure 2, we have performed two additional sets of experiments employing mixtures containing varying amounts of H_2 and CH_4 with the total concentration of the two molecular reactants kept constant.

Figure 6 presents the measured yields of benzene and toluene in comparison with kinetically predicted values. Solid curves, computed at 757 and 866 K with our k_1 as given in Table 4, agree quantitatively with the observed results. The replacement of our k_1 with that of Heckmann et al.[12] leads to noticeable deviation between the predicted values (shown by the dotted curves) and the experimental results under the CH_4-rich condition. This clearly suggests that, although the absolute values of their k_1 in the 1050−1450 K range agree with our theoretically predicted result, the extrapolation of their Arrhenius expression to $T < 1000$ K leads to an overestimate of the rate constant.

B. Ab Initio MO/TST Calculations. *Molecular and Transition State Structures.* The geometries of the reactants, transition state, and products were first optimized at the B3LYP/6-31G(d,p) level and then refined with the 6-311++G(d,p) basis set. The optimized geometries of individual species are presented

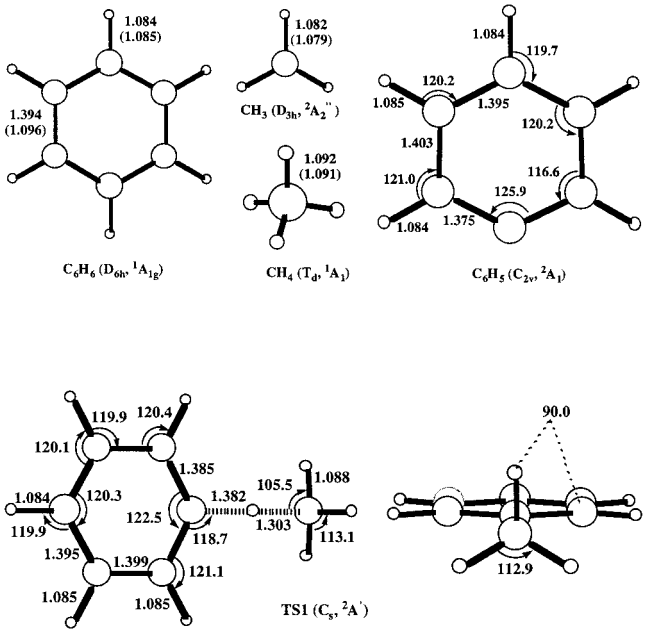

Figure 7. Optimized (B3LYP/6-311++G(d,p)) and experimental (in parentheses) geometries (bond length in Å, angles in deg) of the species involved in the $C_6H_5 + CH_4 \leftrightarrow C_6H_6 + CH_3$ reaction.

in Figure 7. The calculated geometry of benzene is in excellent agreement with the experimental data[31] obtained by making combined use of electron diffraction intensities and rotational constants (r_{av}(C−C) = 1.396 Å, r_{av}(C−H) = 1.085 Å). Calculated C−H bond lengths reproduce the experimental geometry of methane and the methyl radical within the uncertainty of the experimental values.[32] For the local minima, all vibrational frequencies are real. For the transition state, the fully optimized structure (a first-order saddle point characterized by only one imaginary frequency) corresponds to the conformation where the methyl group is twisted out from the C_s-symmetric staggered conformation by ∼4°. To be certain, we carried out the geometry optimization with the constraint of C_s symmetry. The resulting stationary point possessed two imaginary frequencies: one corresponding to the H-abstraction reaction coordinate and the other to the torsional mode. However, the calculated energy difference between the C_1 and C_s structures at the B3LYP/6-31G(d,p) was less than 0.01 kcal/mol and the values of the vibrational frequencies, except that of the torsional mode, differed by less than 0.3 cm^{-1}. A nearly stationary potential energy surface along the torsional coordinate and a very weak dependence of other vibrational modes on it allowed us to neglect conformational effects and use the B3LYP/6-311++G(d,p) optimized staggered conformation for the calculation of refined vibrational frequencies (with the same basis set) and higher level single point energies.

The reaction of the phenyl radical with methane proceeds via an abstraction TS1 with a linear C···H···C fragment. Both the breaking C−H bond between the hydrogen atom and the carbon atom of methyl radical and the forming C−H bond with the carbon atom of phenyl radical are considerably elongated by 0.21 and 0.30 Å, respectively. The length of the breaking bond is shorter than the forming C−H bond by 0.08 Å. The changes of geometrical parameters away from the reaction center are less significant. The C−C bond lengths in the transition state are intermediate between the corresponding values in the phenyl radical and benzene; consequently, the C−C bonds adjacent to the forming C−H bond exhibit the largest change of ∼0.01 Å going either from the reactant or the product. The changes in the geometry of the methyl fragment reflect a transformation of the sp^3-hybridization in methane to sp^2 in the methyl radical, though the structure of the methyl fragment remains sufficiently pyramidal, i.e., closer to the reactants. Thus, the overall structure of the transition state is closer to the reactants, which is in accordance with the exothermicity of the reaction.

It is also worth noting that the phenyl fragment preserves C_{2v} local symmetry, and the local symmetry of the methyl group is very close to C_{3v}. In the preceding discussion we mentioned that conformational effects in the transition state can be neglected for the purpose of vibrational frequencies and energetic parameters calculations. Furthermore, very low absolute values of the torsional frequency (less than 20 cm^{-1}) allowed us to neglect conformational effects and consider it as a free internal rotor for the purpose of the rate constant evaluation.

Other calculated and available experimental vibrational frequencies of the reactants, products, and the transition state are presented in Table 5. In general, B3LYP frequencies reproduce the experimental values much better than those of HF and MP2. Indeed, when calculated with a sufficiently large basis set, B3LYP frequencies agree with experiment so closely that they can be used unscaled for the rate constant calculation. For methane, the calculated frequencies are on average 2.9% higher than the observed[32] ones; the deviations range from 1.6 to 3.7%, which is reasonable due to considerable anharmonicity of CH stretching and bending modes. Similar deviations are seen in the case of the methyl radical,[32] except for the wagging mode whose frequency (580 cm^{-1}) is underestimated by 7.6%. However, this is a much better prediction compared to the value calculated with the 6-31G(d,p) basis set (462 cm^{-1}, about 20% lower than the observed frequency) or at the UMP2/6-311G-(2d,p) level of theory (419 cm^{-1}, about 28% lower).[33] At the latter level the mean absolute deviations (5% for CH_4, 11% for CH_3) are also significantly higher than the ones obtained at the B3LYP/6-311++G(d,p) level (∼3% for both molecules). For the phenyl radical, limited experimental data are available. Only 24 of 27 fundamental modes were observed in the IR spectrum of the phenyl radical trapped in the Ar matrix.[33] Definitive assignments of IR inactive and very weak bands require an additional determination by Raman spectroscopy and studies of isotopomers. The mean absolute deviation of the B3LYP/6-311++G(d,p) calculated from the experimental frequencies of C_6H_5 is 2.8%. Only five theoretical frequencies exceed that assigned from the IR spectrum by more than 3.4%. In fact, one of them (665 cm^{-1}) is predicted to have a medium intensity and lie in the region obscured by CO_2 absorption, whereas Radziszewski et al.[34] assigned to it a very weak band 621 cm^{-1}. The four other frequencies also have very small IR intensities, and their assignment is questionable. The experimental vibrational spectrum of benzene[35] agrees closely with the calculated harmonic frequencies with the mean absolute deviation of 2.2% and maximum deviation ∼4% for C−H stretching modes. Overall, the validity of using unscaled B3LYP/6-311++G(d,p) frequencies is well-supported by their low mean deviations from the available experimental data.

Energetics of the Reaction. H-abstraction reactions by organic radicals play a pivotal role in the propagation and inhibition stages of the chain processes in the hydrocarbon substrates. Several previous studies revealed a general trend in the energetic profile of this elementary action. In particular, the reactions of vinyl and phenyl radicals with molecular hydrogen have been already studied theoretically in our laboratory.[13,36]

TABLE 5: Moments of Inertia[a] (I_A, I_B, I_C), Symmetry Numbers (σ), and Vibrational Frequencies of the Species Involved in the $C_6H_5 + CH_4 = C_6H_6 + CH_3$ Reaction

			frequencies (ν/cm^{-1})	
molecule	I_A, I_B, I_C/10^{-40} g cm^2		calculated[a]	experimental[b]
CH_4	5.36, 5.36, 5.36	A_1	3024	2917
$\sigma = 12$		E	1558	1534
		T_2	1340, 3129	1306, 3019
CH_3	2.95, 2.95, 5.90	A_1	536, 3103	580, 3002
$\sigma = 6$		E	1402, 3283	1383, 3184
C_6H_5	134.34, 150.48, 284.82	A_1	619, 987, 1015, 1049, 1175, 1468, 1571, 3156, 3174, 3187	605, 971, 1011, 1027, 1080 (?), 1441, 1499 (?), 3052, 3071, 3085
$\sigma = 2$		A_2	398, 812, 962	402, 818, 961
		B_1	424, 665, 718, 892, 984	416, 621 (?), 708, 878, 976
		B_2	600, 1072, 1176, 1302, 1325, 1461, 1625, 3162, 3177	586, 1067, 1086 (?), 1226 (?), 1344, 1433, 1593, 3060, 3073
C_6H_6	148.20, 148.20, 296.40	A_{1g}	1011, 3191	993, 3074
$\sigma = 12$		A_{2g}	1381	1350
		A_{2u}	684	674
		B_{1u}	1022, 3155	1010, 3057
		B_{2g}	719, 1010	707, 990
		B_{2u}	1175, 1337	1150, 1309
		E_{1g}	861	849
		E_{1u}	1059, 1511, 3181	1038, 1484, 3057
		E_{2g}	622, 1198, 1634, 3165	608, 1178, 1610, 3050
		E_{2u}	409, 979	398, 967
TS1[a]	Overall	A′	1551i, 87, 360, 403, 508, 671, 695, 733, 906, 992, 1012, 1027, 1063, 1186, 1189, 1270, 1444, 1495, 1597, 3052, 3151, 3165, 3177, 3184	
	154.77, 508.39, 657.59	A″	90, 398, 531, 619, 841, 967, 1079, 1178, 1301, 1326, 1378, 1448, 1483, 1625, 3155, 3170, 3175	
	Internal[c]			
$\sigma = 6$	5.51			

[a] Calculated at the B3LYP/6-311++G(d,p) level. [b] Experimental frequencies are from ref 32 (CH_3 and CH_4), 34 (C_6H_5), and 35 (C_6H_6). [c] $-CH_3$ rotor.

TABLE 6: Total Energies (in Hartree) and ZPE (in kcal/mol) of the Reactants and Relative Energies (ZPE Corrected, in kcal/mol) of the TS1 and Products Calculated at Various Levels of Theory

species	$C_6H_5 + CH_4$	TS1[a]	$C_6H_6 + CH_3$[a]
$\langle S^2 \rangle$ (UHF/6-311G(d,p))	1.38	1.38	0.76
$\langle S^2 \rangle$ (B3LYP)	0.76	0.76	0.75
ZPE (B3LYP/6-311++G(d,p)	82.50	80.25	81.39
B3LYP/6-31G(d,p)[b]	−272.09324	7.26	−6.29
B3LYP/6-311++G(d,p)	−272.156336	8.04	−7.48
B3LYP/6-311++G(3df,2p)	−272.175468	8.33	−7.35
MP2/6-311G(d,p)	−271.23509	9.99	−32.41
MP2/6-311+G(3df,2p)	−271.40109	9.29	−32.99
PMP4/6-31G(d,p)	−271.28086	9.63	−11.59
PMP4/6-311G(d,p)	−271.37098	8.13	−12.03
CCSD/6-31G(d,p)	−271.24346	12.87	−9.60
CCSD(T)/6-31G(d,p)	−271.28334	11.33	−9.41
CCSD/6-311G(d,p)	−271.32758	11.65	−9.93
CCSD(T)/6-311G(d,p)	−271.37240	9.97	−9.72
G2M (cc,MP2)	−271.50250	9.14	−10.43
G2M (CC, MP2)	−271.50594	**9.27**	**−10.30**

[a] Energies relative to the reactants. [b] B3LYP/6-31G(d,p)//B3LYP/6-31G(d,p). ZPE(B3LYP/6-31G(d,p)) for the reactants, TS1, and products are 83.13, 80.81, and 81.78 kcal/mol, respectively.

The heat of the H-abstraction reaction is determined by the strengths of the breaking and forming bonds; in the present study these are C−H bonds in methane and benzene, respectively. As pointed out by Mebel et al.,[13] the UHF wave function for the phenyl radical is highly spin contaminated (see Table 6). Hence, methods not taking into account high-order correlation energy (UHF, MP2) overestimate the energy of the phenyl radical and consequently the C−H bond energy in benzene. For this reason, the MP2 values for the heat of the H-abstraction reactions by C_6H_5 contain a large, but systematic error. On the contrary, the B3LYP calculation of the phenyl radical produces a wave function that is almost a pure doublet with $\langle S^2 \rangle = 0.76$. The B3LYP estimate of the $C_6H_5 + CH_4 = C_6H_6 + CH_3$ reaction exothermicity (−7.5 kcal/mol) is close to the values obtained by such methods as PMP4, CCSD, and CCSD(T) that take into account the higher order correlation effects (Table 6). The experimental C−H bond strengths are $D_0(CH_3-H) = 103.2 \pm 0.3$ kcal/mol in methane[32] and $D_0(C_6H_5-H) = 112.0 \pm 0.6$ kcal/mol in benzene.[37] The best agreement with the experimental value of $\Delta H_0^0 = -8.8 \pm 0.9$ kcal/mol is the CCSD(T) values (9.4 and 9.7 kcal/mol with the double- and triple-ζ basis sets, respectively). The fourth-order perturbation calculation (MP4) significantly improves the MP2 values, yet the exothermicity of the reaction is still overestimated by ∼3 kcal/mol. The experimental ΔH_0^0 differs by only 1.5 kcal/mol from that calculated at the G2M(CC,MP2) level. The difference is similar to that found for the analogous reaction, $C_6H_5 + H_2 = C_6H_6 + H$.[13] The error results essentially from the overestimate of the C−H bond energy in benzene by the G2M schemes.

For the $C_6H_5 + CH_4 = C_6H_6 + CH_3$ reaction, we possess nearly complete experimental data (vibrational frequencies of the reactants and products, geometries of methane, the methyl radical, and benzene, and ΔH_0^0 of the reaction) necessary for the equilibrium constant evaluation. Using calculated moments of inertia and vibrational frequencies for benzene and the phenyl radical and experimental values of all other parameters, we obtained the T dependent Gibbs free energy change in this reaction and the equilibrium constant. Thus the calculated equilibrium constant is best expressed in the form

$$K_1 = (2.85 \pm 0.42) \times 10^{-2} T^{0.34 \pm 0.02} \exp(4438.2 \pm 16.1/T) \quad \text{(III)}$$

Because the deviations of our theoretical molecular parameters from the available experimental ones are very small, the

equilibrium constant calculated solely from theoretical moments of inertia and vibrational frequencies and the experimental ΔH_0^0 of the reaction differs from that given in eq III by only 14% at 2000 K and by less than 10% in the temperature range 298−1000 K.

In the calculation of the activation barrier height a similar problem caused by the high spin contamination can be expected, since the UHF wave function for the transition state has $\langle S^2 \rangle = 1.38$, much higher than that expected for a proper doublet. However, this value matches the $\langle S^2 \rangle$ value for the phenyl radical. This is not surprising because the forming C_6H_5-H bond in the transition state is very weak and the structure of the phenyl fragment resembles the structure of the free phenyl radical. The implication of this structural similarity between the reactants and the transition state is the cancelation of errors in the theoretically predicted barrier height for the forward reaction. Naturally, the MP2 energies for the transition state relative to the reactants are consistent with those calculated at higher levels (Table 6). On the other hand, the barrier for the reverse reaction should be corrected for the error in the enthalpy of this reaction resulting from the unbalanced accuracy of the calculated energies for the reactants and products. Since the source of error is the overestimated energy of the phenyl radical, the correction is equivalent to the downward shift in the energy of the reactants and the transition state relative to the energy of the products. The calculated barrier height at our best level (G2M(CC,MP2)) for the forward reaction, 9.3 kcal/mol, is close to the earlier reported theoretical barriers for the $C_6H_5 + H_2 \rightarrow C_6H_6 + H$ (8.8 kcal/mol)[13] and $C_2H_3 + H_2 \rightarrow C_2H_4 + H$ (10.4 kcal/mol)[36] reactions, both obtained at the G2M(rcc,MP2) level of theory. The barrier for the reverse reaction corrected to reproduce the enthalpy of the reaction is 18.1 kcal/mol (at the G2M(CC,MP2) level). The activation energies calculated by the B3LYP method are somewhat lower than the G2M values. We suppose that the stability of the transition state structure is overestimated in B3LYP calculations. This appears to be a typical error of density functional methods that they overestimate the stability of weakly bound systems[38,39] despite the ability to generate high-quality geometries. In particular, for the reactions involving a hydrogen atom, hybrid DFT methods compute activation energies that are 2−3 kcal/mol less than the experimental values.[38] However, the basis set expansion appears to cause an increase in the B3LYP barrier heights, thus, approaching the G2M predictions.

Rate Constant Calculations. The bimolecular rate constant for the $C_6H_5 + CH_4$ reaction was computed with the canonical transition state theory (CTST) with Eckart quantum mechanical tunneling corrections[40] (see Appendix I) using the molecular parameters and energies presented in Tables 5 and 6, respectively. The moments of inertia and unscaled harmonic vibrational frequencies obtained at the B3LYP/6-311++G(d,p) level of theory were employed for the rate constant calculation. The transition state has three low vibrational frequencies that correspond to the methyl−phenyl torsional mode ($|\nu| < 20$ cm^{-1}) and the two nearly degenerate C−H−C bending modes in and out of the phenyl plane as illustrated in Figure 8. For the rate constant calculation, the former was treated as a free internal rotor, whereas the latter two modes were treated either as harmonic oscillators or a 2-D hindered rotor. For the 2-D hindered rotor calculation, we employed the method used by Hase and Zhu.[41] The predicted rate constants by the two models agree closely for the temperatures below 2500 K. As shown in Figure 2, all experimental data, except those of Duncan and Trotman-Dickenson,[15] could be reasonably accounted for by the theory with the energy barrier $E_1^0 = 10.5 \pm 0.5$ kcal/mol: $k_1 = 3.89 \times 10^{-3} T^{4.57} \exp(-2645/T)$ cm^3/(mol s), which is valid for the temperature range 300−2500 K. The energy barrier that fits all the experimental data is well within the 2−3 kcal/mol accuracy of the predicted best values of 9.1−10.0 kcal/mol.

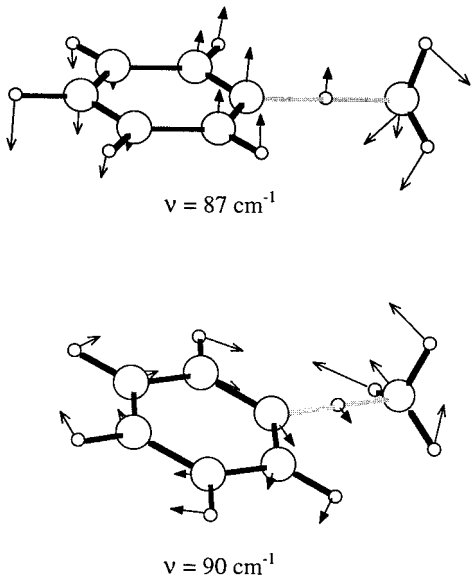

Figure 8. Low-frequency bending vibrations of the transition state calculated at the B3LYP/6-311++G(d,p) level of theory. The vectors shown are proportional to the actual displacement.

On the treatment of the two nearly degenerate bending vibrations, we have also examined its hypothetical (maximal) effect on the predicted rate constant by considering a 2-D free internal rotor model. In this treatment, the reduced moment of inertia of the 2-D rotor (5.8×10^{-40} g cm^2) was evaluated using the calculated moments of inertia ($I_x \approx I_y$) of the C_6H_5 and CH_4 fragments of the TS1. The contribution of the corresponding vibrational modes into ZPE (∼0.25 kcal/mol) was removed before substituting the calculated activation energy in the CTST expression for the rate constant. The result of this calculation with the same energy barrier ($E_1^0 = 10.5$ kcal/mol) showed that the value of k_1 increased by a factor of 6.0 at 500 K and decreased by a factor of 1.1 at 2000 K.

5. Conclusion

In this work we have investigated experimentally and theoretically the reaction of the phenyl radical with methane. The rate constant for the bimolecular metathetical reaction measured with the combination of pyrolysis/FTIR spectrometry and pulsed laser photolysis/mass spectrometry techniques covering the temperature range 600−980 K can be presented by the equation: $k_1 = 10^{12.78} \exp(-6201/T)$ cm^3/(mol s). The rate constant k_1 calculated from theoretical molecular parameters fits our experimental data and also the result of the high-temperature shock-tube/UV absorption measurement by Heckmann et al.[12] if the energy barrier $E_1^0 = 10.5$ kcal/mol is used. This value is close to $E_1^0 = 9.3$ kcal/mol obtained at our highest theoretical level, G2M(CC, MP2)//B3LPYP/6-311++G(d,p). For the purpose of high-temperature kinetic modeling, the expression, $k_1 = 3.89 \times 10^{-3} T^{4.57} \exp(-2645/T)$ cm^3/(mol s), obtained from the calculation is recommended for the temperature range 300−2500 K. From the analysis of the toluene formation data with and without added H_2 and CH_4, we have obtained very reproducibly the rate constant for the recombination of CH_3 with C_6H_5, $k_2 = (1.38 \pm 0.08) \times 10^{13} \exp[-(23 \pm 46)/T]$ cm^3/(mol s) for the temperature range 300−980 K.

Acknowledgment. The authors are grateful for the support of this work from the Basic Energy Sciences, Department of Energy, under contract no. DE-FG02-97-ER14784. We are also thankful to Dr. W. H. Kirchhoff for providing us sufficient NERSC CPU time for the lengthy ab initio MO calculations.

Appendix I. Eckart Tunneling Correction Calculation

To calculate the tunneling effect correction, the barrier along the reaction coordinate x was approximated by the unsymmetric three-parameter Eckart potential[40]

$$V(x) = \frac{e^u}{1+e^u}\left(E_1 - E_{-1} + \frac{(\sqrt{E_1} + \sqrt{E_{-1}})^2}{1+e^u}\right)$$

where $u = 2\pi x/l$. The constants $E_1 = 10.5$ kcal/mol and $E_{-1} = 19.3$ kcal/mol represent the barrier heights relative to reactants and products, respectively. The third parameter l is chosen to reproduce the curvature of an ab initio potential at the maximum

$$V''(x) = -\frac{8\pi^2}{l^2}(E_1{}^{-1/2} + E_{-1}{}^{-1/2})^{-2} = -4\pi^2\mu|\nu^*|^2$$

where $\nu^* = i1551\ cm^{-1}$ is the imaginary frequency and μ is the reduced mass of the tunneling hydrogen. Solving the appropriate one-dimensional Shrödinger equation,[40] we obtain the tunneling probability for an incident particle of mass μ and energy E

$$P(E) = \frac{\cosh[2\pi(\alpha+\beta)] - \cosh[2\pi(\alpha-\beta)]}{\cosh[2\pi(\alpha+\beta)] + \cosh[2\pi\delta]}$$

with $\alpha = (2\mu l^2 E/h^2)^{1/2}$, $\beta = ([2\ \mu l^2(E - (E_1 - E_{-1}))]/h^2)^{1/2}$, and $\delta = ((4E_1E_{-1}/h|\nu^*|^2) - (1/4))^{1/2}$. Integration of the energy specific probability over a Maxwell−Boltzmann distribution yields the tunneling correction for the transition state theory rate constant

$$Q = \frac{1}{RT}\int_0^\infty P(E)\exp\left(-\frac{E-E_1}{RT}\right)dE$$

References and Notes

(1) Yu, T.; Lin, M. C. *J. Am. Chem. Soc*. **1993**, *115*, 4371.
(2) Yu, T.; Lin, M. C.; Melius, C. F. *Int. J. Chem. Kinet.* **1994**, *26*, 1095.
(3) Yu, T.; Lin, M. C. *J. Am. Chem. Soc*. **1994**, *116*, 9571.
(4) Yu, T.; Lin, M. C. *Combust. Flame* **1995**, *100*, 169.
(5) Yu, T.; Lin, M. C. *J. Phys. Chem*. **1995**, *99*, 8599.
(6) O'Keefe, A.; Deacon, D. A. G. *Rev. Sci. Instrum.* **1988**, *59*, 2544.
(7) Park, J.; Lin, M. C. ACS Symposium Series 720 on Cavity-Ringdown Spectroscopy; American Chemical Society: Washington, DC, 1999; Chapter 13.
(8) Park, J.; Lin, M. C. *J. Phys. Chem. A* **1997**, *101*, 14.
(9) Park, J.; Dyakov, I. V.; Lin, M. C. *J. Phys. Chem. A* **1997**, *101*, 8839.
(10) Wyatt, J. R.; DeCorpo, J. J.; McDowell, W. V.; Saalfeld, F. E. *Rev. Sci. Instrum*. **1974**, *45*, 916.
(11) Wyatt, J. R.; DeCorpo, J. J.; McDowell, M. V.; Saalfeld, F. E. *Int. J. Mass Spectrom. Ion Phys*. **1975**, *16*, 33.
(12) Heckmann, E.; Hippler, H.; Troe, J. *Symp. (Int.) Combustion, 26th* **1996**, 543.
(13) Mebel, A. M.; Lin, M. C.; Yu, T.; Morokuma, K. *J. Phys. Chem. A* **1997**, *101*, 3189.
(14) Mebel, A. M.; Morokuma, K.; Lin, M. C. *J. Chem. Phys*. **1995**, *103*, 7414.
(15) Duncan, F. J.; Trotman-Dickenson, A. F. *J. Chem. Soc*. **1962**, 4672.
(16) Becke, A. D. *J. Chem. Phys*. **1993**, *98*, 5648. (b) Becke, A. D. *J. Chem. Phys*. **1992**, *96*, 2155. (c) Becke, A. D. *J. Chem. Phys*. **1992**, *97*, 9173.
(17) Lee, C.; Yang, W.; Parr, R. G. *Phys. Rev. B* **1988**, *37*, 785.
(18) Pople, J. A.; Head-Gordon, M.; Raghavachari, K. *J. Chem. Phys.* **1987**, *87*, 5768.
(19) Laidler, K. J. *Chemical Kinetics*, 3rd ed.; Harper and Row: New York, 1987.
(20) Frisch, M. J.; Trucks, G. W.; Schlegel, H. B.; Gill, P. M. W.; Johnson, B. G.; Robb, M. A.; Cheeseman, J. R.; Keith, T.; Petersson, G. A.; Montgomery, J. A.; Raghavachari, K.; Al-Laham, M. A.; Zakrzewski, V. G.; Ortiz, J. V.; Foresman, J. B.; Cioslowski, J.; Stefanov, B. B.; Nanayakkara, A.; Challacombe, M.; Peng, C. Y.; Ayala, P. Y.; Chen, W.; Wong, M. W.; Andres, J. L.; Replogle, E. S.; Gomperts, R.; Martin, R. L.; Fox, D. J.; Binkley, J. S.; Defrees, D. J.; Baker, J.; Stewart, J. P.; Head-Gordon, M.; Gonzalez, C.; Pople, J. A. *GAUSSIAN 94*, Revision D.3; Gaussian, Inc.: Pittsburgh, PA, 1995.
(21) Luts, A. E.; Lee, R. K.; Miller, J. A. SENKIN: A FORTRAN Program for Predicting Homogeneous Gas-Phase Chemical Kinetics with Sensitivity Analysis; Sandia National Laboratories Report No. SANDIA 89-8009, **1989**.
(22) Yu, T.; Lin, M. C. *J. Phys. Chem*. **1994**, *98*, 2105.
(23) Park, J.; Dyakov, I. V.; Mebel, A. M.; Lin, M. C. *J. Phys. Chem. A* **1997**, *101*, 6043.
(24) Horn C.; Frank P.; Transter, R. S.; Schaugg, J.; Grotheer, H.-H.; Just. T. *Symp. (Int.) Combustion*, *26th* **1996**, 575.
(25) Tsang, W.; Kiefer, J. H. In *The Chemical Dynamics and Kinetics of Small Radicals*; Liu, K., Wagner, A. F., Eds.; World Scientific: Singapore, 1996; Part I, p 58.
(26) Park, J.; Chakraborty, D.; Bhusari, D. M.; Lin, M. C. *J. Phys. Chem. A*, in press.
(27) Krech, M.; Price, J. W. *Can. J. Chem*. **1967**, *45*, 157.
(28) Zhang, H.-X.; Ahonkhai, S. I.; Back. M. H. *Can. J. Chem*. **1989**, *67*, 1541.
(29) NIST Chemical Kinetics Database, 1998, 2Q98.
(30) Tokmakov, I. V.; Lin, M. C. To be published.
(31) Cabana, A.; Bacchand, J.; Giguere, J. *Can. J. Phys*. **1974**, *52*, 1949. (b) Tamagawa, K.; Iijima, T.; Kimura, M. *J. Mol Struct*. **1976**, *30*, 243.
(32) Chase, M. W., Jr.; Davles, C. A.; Downey, J. R., Jr.; Frurip, D. J.; McDonald, R. A.; Syverud, A. N. JANAF Thermochemical Tables. *J. Phys. Chem. Ref. Data* **1985,** *14,* Suppl. 1.
(33) Truong, T. N.; Truhlar, D. G. *J. Chem. Phys*. **1990**, *93*, 1761.
(34) Radziszewski, J.; Nimloss, M. R.; Winter, P. R.; Ellison, G. B. *J. Am. Chem. Soc*. **1996**, *118*, 7400.
(35) Snels, M.; Beil, A.; Hollenstein, H.; Quack, M. *Chem. Phys*. **1997**, *225*, 107−130.
(36) Mebel, A. M.; Diau, E. W. G.; Lin, M. C.; Morokuma, K. *J. Am. Chem. Soc*. **1996**, *118*, 9759.
(37) Davico, G. E.; Bierbaum, K.; DePuy, C. H.; Ellison, G. B.; Squires, R. S. *J. Am. Chem. Soc*. **1995**, *117*, 2590.
(38) Jursic, B. C. *J. Mol. Struct*. **1997**, *417*, 89.
(39) Johnson, B. J.; Gonzales, C. A.; Gill, P. M. W.; Pople, J. A. *Chem. Phys. Lett*. **1994**, *221*, 100.
(40) Eckart, C. *Phys. Rev*. **1930**, *35*, 1303.
(41) Hase, W. L.; Zhu, L. *Int. J. Chem. Kinet*. **1994**, *26*, 407.